An interfacial area generation study for multi-component fluid mixing

P.D. Anderson, O.S. Galaktionov, P.G.M. Kruijt,
F.N. van de Vosse, G.W.M. Peters, and H.E.H. Meijer
Eindhoven University of Technology, Materials Technology,
PO Box 513, NL-5600 MB Eindhoven,
The Netherlands.

March 1, 1999

Abstract

Mixing simulations of chaotic flows usually start from the point that mixing of a single fluid is considered. The exponential increase of interfacial area in these chaotic systems calls for sophisticated numerical algorithms to simulate initial stages of mixing. Because of the enormous increase in computer power during the last years, these computational techniques have been successfully applied to obtain a better understanding of two– and three-dimensional chaotic mixing flows. A natural next step is to study systems with multiple fluid components. Here a computational technique is presented to study multi-component mixing in two– and three-dimensional systems. Because a separate (fixed) mesh is used for the flow domain and a variable adaptive mesh for the fluid interfaces, systems can be studied with an exponential increase of interfacial area. In particular, the influence of viscosity ratio and interfacial tension on the generation of interfacial area is studied in some prototypical mixing flows.

1 Introduction

Investigation of chaotic mixing in two– and three-dimensional flows in cavities has been described in the literature see for example Ottino (1989), Chien *et al.* (1986), Liu *et al.* (1994), Anderson *et al.* (1999), Aref (1984), Ashwin and King (1997), Carey and Chen (1995) and references within. Much of this work, and other studies, is done to elucidate fundamental kinematics of mixing processes with passive interfaces. In contrast to these studies, this paper reports on the mixing of two dissimilar (immiscible) fluids. They can have different viscosities, and interfacial tension can become important. Here the interfaces are not passively advected in the flow, but they modify the flow within both phases.

Numerical simulations of morphological evaluation in chaotic mixing involve the solution of the Navier−Stokes equations for two or more fluid phases with specified boundary and interfacial conditions. An important difficulty in those numerical simulations is the unknown position of the moving interface, which must be found together with the velocity and pressure fields in the fluid phases. Several approaches to solve these types of problems are available in the literature, although only a few have been applied to investigate chaotic mixing problems. Zhang and Zumbrunnen (1996a) studied the influence of mixing of two similar fluids by a third dissimilar fluid. Regions of regular motion (islands) can be destroyed by the influence of the third fluid. Their results suggest that mixing can be promoted by the presence of a dissimilar fluid. In another study Zhang and Zumbrunnen (1996b) examined the formation of fine-scale structures which are influenced by interfacial tension. Chella and Viñals (1996) introduced a numerical technique where a diffuse interface model was used to study mixing in cavities. Advection of two fluids which are horizontally layered in a lid-driven cavity was studied as a function of capillary forces, and the results were compared to the classical case of a passively advected

interface. They found, in cases where surface tension is important, that the interfacial stretch is less than the stretch for a passively advected interface. Chakravarthy and Ottino (1996) studied mixing in a square cavity and considered the influence of viscosity ratio on the generation of interfacial area. Different mixing parameters, where the viscosities of the two fluids are of the same order, and two different initial configurations were considered. They reported that if the disperse phase has a lower viscosity, more stretching along the interface occurs, however, in this study the influence of interfacial tension was neglected.

2 Direct numerical simulation of multi-component fluid mixing

If the effect of interfacial tension on a fluid interface is considered, the surface stress boundary conditions at an interface between two fluids (labeled "1" and "2") is Landau and Lifshitz (1959) often denoted as

$$(p_1 - p_2 + \sigma\kappa)\boldsymbol{n}_i = (\boldsymbol{\tau}_{1ik} - \boldsymbol{\tau}_{2ik})\boldsymbol{n}_k + \frac{\partial\sigma}{\partial x_i}, \tag{1}$$

where σ is the fluid surface tension coefficient, p_α is the pressure in fluid α, and $\boldsymbol{\tau}_{\alpha ik}$ is the viscous stress tensor in fluid α. In equation (1) the Einstein summation convention is used. The vector $\boldsymbol{n}_i$ is the unit normal (into fluid "2") at the interface, and κ is the local surface curvature. The capillary number, which measures viscous forces relative to interfacial forces, follows from equation (1). Let $1/L$ measure the curvature κ and $\eta\dot{\gamma}$ be a scale for the viscous forces. Then the capillary number can be defined as

$$Ca = \frac{\eta\dot{\gamma}}{\sigma/L} = \frac{\eta\dot{\gamma}L}{\sigma}. \tag{2}$$

In general the surface tension σ may vary along the interface, but here only the modelling of viscous incompressible fluids with a constant surface tension coefficient is considered. This condition reduces equation (1) to Laplace's formula Landau and Lifshitz (1959) for the surface pressure p_s, the fluid pressure jump across an interface under surface tension:

$$p_s \equiv p_2 - p_1 = \sigma\kappa. \tag{3}$$

The surface pressure is therefore proportional to the curvature κ of the interface. The surface force per unit interfacial area can be written as

$$\boldsymbol{F}_s = \sigma\kappa(\boldsymbol{x}_s)\boldsymbol{n}(\boldsymbol{x}_s), \tag{4}$$

where $\kappa(\boldsymbol{x}_s)$ is the curvature, taken positive if the centre of curvature is in fluid "2" Brackbill *et al.* (1992), and $\boldsymbol{n}(\boldsymbol{x}_s)$ is the unit normal to the interface at $\boldsymbol{x}_s$, assumed to point into fluid "2".

Most of the existing numerical methods for multi-phase flows fall into one of the following three categories: those which use a fixed grid, those which allow the grid to deform in time so that it remains surface intrinsic, and those which use a fixed grid to represent the flow field and a separate moving grid to represent the interface. In the first category an additional variable is used to identify the interface and examples are the *marker and cell* (MAC) method Harlow and Welch (1965) and the *volume of fluid* (VOF) method by Hirt and Nichols (1981). The most difficult task within these approaches is to accurately define the interface and to impose the interface condition (1). This difficulty can be alleviated by using a *continuum surface force* (CSF) method proposed by Brackbill *et al.* (1992). When the CSF model is used, the interface condition (1) is put in the momentum equations rather than being imposed explicitly at the interface. A combination of the VOF method and the CSF model has been used

by a number of authors to simulate multi-phase phenomena. An advantage of this combination is the possibility to model complex topological changes. A different approach, also within the first category, is based on the idea that the interface has a non-zero thickness (i.e., it is diffuse), and uses gradient theories for the interface based on thermodynamic principles. See for example Chella and Viñals (1996), Verschueren (1999), and Anderson *et al.* (1998) and references therein for an overview of these methods and their application. For methods in the second category, imposing the interface condition (1) is easy compared with the first, because the interface always coincides with boundaries of mesh elements. However, this approach requires frequent updating of the computational mesh, which can be a complex and time-consuming procedure. For small deformations a fixed mesh topology can be kept and only updating of the nodal points is required. For larger deformations the mesh is distorted such that re-meshing of the full flow domain is necessary. This model also encounters severe difficulties with complex topological changes.

The third approach is based on a combination of mixed and moving grids. Unverdi and Tryggvason (1992b) explicitly tracked the interface, which is kept at a constant thickness at the order of the mesh element size of the flow domain. Convection equations are used to update the density and viscosity, and some specific treatment to the front avoids oscillations at the interface.

The model introduced in this paper falls into the third category and differs from the method of Unverdi and Tryggvason (1992b) in the way surface tension forces are incorporated. In their computations they included the surface tension from the curvature of the interface using equation (4). In this paper surface tension is included using its definition (Batchelor, 1967) directly: across any line drawn on the interface a force of magnitude σ per unit length is exerted in a direction normal to the line and tangential to the interface.

2.1 Methods to track deforming fluid elements

The tracking of material interfaces in fluid flows is widely addressed in the literature. Several techniques developed for tracking were reviewed by Beris *et al.* (1996), Hyman (1984), Rudman (1997), and Unverdi and Tryggvason (1992a). Without repeating these reviews, it should be mentioned that in general there are two basic approaches: *front capturing* and *front tracking*.

Well-known *front capturing* methods are the simplified line interface calculation (SLIC, Noh and Woodward (1976)), the volume of fluid method (VOF, Hirt and Nichols (1981)), and the method of Young Young *et al.* (1980). In case of front capturing, markers are distributed over the fluid volume, or a special marker function is passively advected with the flow. In this case special techniques are used to restore ("capture") the shape of the interface, using the computed values of the marker function. The advantages of this approach are a relatively simple formulation for the advection of the marker function and the ability to deal with interaction of interfaces with relative ease. The drawback of front capturing is the complexity of the interface shape restoration techniques, which frequently (especially in the three-dimensional case) have difficulties restoring a smooth and continuous surface, see (Rudman (1997), and Qu and Li (1996)).

Within a *front tracking* approach a separate moving mesh is used to describe the interface. Front tracking allows sub-grid resolution; the interface position is known with a higher precision than the size of the elements used for main flow computation. A front tracking method does not suffer from disadvantages that result in erroneously non-smooth or discontinuous surfaces. A disadvantage of front tracking is the difficulty of describing topological changes like breakup and coalescence. However, front tracking can account for surface-related forces like surface tension. Galaktionov *et al.* (1999) compared front tracking and front capturing for a mixing shear-layer problem. The results showed that front tracking provides more detailed layered structures.

In this work a surface is described by an unstructured triangular mesh, as done by Tryggvason and Unverdi (1990), and Unverdi and Tryggvason (1992a),Unverdi and Tryggvason (1992b). Additional to their techniques, surface curvature is used here to decide about necessary mesh refinements. Local mesh refinement provides the possibility to use small elements in strongly curved zones of the surface (near sharp edges, for example), and much larger elements in relatively planar zones, keeping the number of elements as low as possible. This significantly reduces the amount of computational work for tracking the moving nodal points. Also the pre-history of the surface deformation is used for adding new markers during mesh refinement. New markers are added on a less deformed, earlier configuration of the surface and then tracked to their current position. This allows the use of simpler linear interpolation. Without history, higher order interpolation is required (see Hyman, 1984).

The mesh data that needs to be stored consists of the list of nodal points, with their coordinates and the information about their connectivity. Both closed and non-closed surfaces, and surfaces consisting of separate segments, can be described as one single object. The elementary objects used by the algorithm to describe the surface are cells (triangles), edges (sides of triangles), and nodes. Thus, three lists are kept. For all nodal points the coordinates are stored. Integer arrays are used to establish relations between basic objects. The first array establishes relations between the cells and nodes, providing the pointers for every triangle to its vertices (nodes). Another array links cells to their edges (three for each cell). Edges, in turn, are referred to via their two end nodes. This scheme of reference is redundant, as, for example, the reference to the vertices of a triangle could be recovered from the edges and their pointers to the nodes. Such redundancy, however, simplifies the algorithms of mesh refinement and restructuring. As any edge belongs to one or two triangles, an additional array refers the edges to the cells they belong to. If only one pointer to a triangle is stored for a certain edge, it serves as indication that this edge belongs to the the contour (boundary) of the surface. This is used during mesh restructuring, preventing the contour shape from being distorted. The last array, referring edges to triangles, is easily re-created in a single loop over all triangles, using the other pointer arrays. It is updated after mesh restructuring and refinement. Its main use is finding which neighbouring triangular cells that share a common edge.

The mesh can become significantly distorted during flow and should be refined where necessary. The most important part of mesh refinement is contained in the choice of the criteria that define whether cells should be refined. The mesh refinement algorithm proposed here is controlled by three parameters :

- h_{max} - the maximum cell edge length.
- $h_{max,\,c}$ - the maximum length of an edge of a cell adjacent to an angle sharper than α_{max}.
- α_{max} - the critical angle between cells. (The angle between neighbouring cells is defined as the angle between their outer normals.)

Thus, the refinement algorithm takes into account the curvature of the surface, so that strongly curved parts of the surface are covered by small cells while relatively flat zones of the surface are described by large cells. This minimizes the number of markers and, thus, the computational expenses.

The mesh edges that are tagged for refinement are split into two edges by adding new nodal points. Figure 1 illustrates how a single triangular cell is transformed when one, two or three of its edges were tagged for refinement. After the mesh refinement is completed, local changes of the mesh topology (re-connection of the nodes) are performed on selected cells.

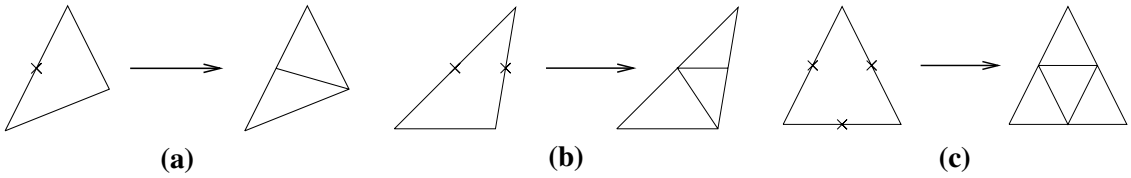

Figure 1: Scheme of transformation of a mesh cell with 1, 2, or 3 edges tagged for refinement.

2.1.1 Parallelization

For a strongly deforming fluid volume in a flow, a large, varying number of markers needs to be tracked. This tracking makes parallel processing attractive because these computations are independent for every point. For the implementation of the parallel algorithm, a master-slave scheme with the dynamical workload distribution over slave processes in a PVM-network (Geist *et al.*, 1994) was chosen. The master program performs all types of mesh transformations and distributes the extensive computational work (time integration) among slaves. An auxiliary program is used to handle the velocity field data, broadcasting it to slaves on request of the master program. More details about the parallel algorithm and its efficiency can be found in Galaktionov *et al.* (1997).

2.2 Velocity field computation

In this section a computational method for flow of two dissimilar (immiscible) Newtonian fluids including surface tension forces is described. The model is such that it can be easily generalised for non-Newtonian mixtures of multiple fluids. For this system the conservation equations of mass and momentum are written as

$$\begin{aligned} \rho(\frac{\partial \boldsymbol{u}}{\partial t} + \boldsymbol{u}\cdot\nabla\boldsymbol{u}) &= -\nabla p + \nabla\cdot 2\eta(\boldsymbol{x},t)\boldsymbol{D} + \boldsymbol{F}_s \\ \nabla\cdot\boldsymbol{u} &= 0, \end{aligned} \tag{5}$$

where $\boldsymbol{F}_s$ denotes the surface tension forces per unit volume. The equations above are scaled using a characteristic velocity U, length scale L, and time ω:

$$\boldsymbol{u}^* = \boldsymbol{u}/U \qquad x^* = x/L \qquad t^* = \omega t \qquad p^* = p/\rho U^2, \tag{6}$$

and surface tension is scaled as $\boldsymbol{F}_s^* = \boldsymbol{F}_s/f_0$, resulting, after dropping the stars, in

$$St\frac{\partial \boldsymbol{u}}{\partial t} + \boldsymbol{u}\cdot\nabla\boldsymbol{u} = -\nabla p + \frac{1}{Re}\nabla\cdot 2\eta(\boldsymbol{x},t)\boldsymbol{D} + \frac{f_0 L}{\rho U^2}\boldsymbol{F}_s \tag{7}$$

$$\nabla\cdot\boldsymbol{u} = 0. \tag{8}$$

The dimensionless Reynolds and Strouhal numbers

$$Re = \rho\frac{UL}{\eta}, \qquad St = \frac{L\omega}{U} \tag{9}$$

are then defined accordingly. The capillary number can now be defined as the ratio of viscous forces versus surface tension forces,

$$Ca = \frac{1/Re}{\frac{f_0 L}{\rho U^2}} = \frac{U\eta}{f_0 L^2}, \tag{10}$$

and also following from (2) $f_0 = \sigma/L^2$, where σ is the surface tension coefficient. Equation (8) can then be formulated as

$$St\frac{\partial \boldsymbol{u}}{\partial t} + \boldsymbol{u}\cdot\nabla\boldsymbol{u} = -\nabla p + \frac{1}{Re}\nabla\cdot 2\eta(\boldsymbol{x},t)\boldsymbol{D} + \frac{1}{Re\ Ca}\boldsymbol{F}_s \tag{11}$$

$$\nabla\cdot\boldsymbol{u} = 0, \tag{12}$$

In equation (5) the viscosity is a function of space and time, and requires updating each time step. It will be described below how the surface tension forces are computed and included as a volume force function. Within this model two meshes are used; one which is fixed and used for the discretization of the fluid domain, and another one which is allowed to deform and which is used to track the fluid interfaces. Applying the second-order backward differences scheme to equation (5) gives

$$\begin{aligned} St\ \frac{3\boldsymbol{u}^{n+1} - 4\tilde{\boldsymbol{u}}^n + \tilde{\boldsymbol{u}}^{n-1}}{2\Delta t} &= -\nabla p^{n+1} + \frac{1}{Re}\nabla\cdot 2\eta^{n+1}\boldsymbol{D}_{\boldsymbol{u}^{n+1}} + \frac{1}{Re\ Ca}\boldsymbol{F}_s^{n+1}, \\ \nabla\cdot\boldsymbol{u}^{n+1} &= 0, \end{aligned} \tag{13}$$

where $\boldsymbol{D}_{\boldsymbol{u}^{n+1}} = \frac{1}{2}(\nabla\boldsymbol{u}^{n+1} + (\nabla\boldsymbol{u}^{n+1})^T)$.
The projection scheme now proceeds as follows:

- A predictor $\boldsymbol{u}_p^{n+1}$ for the velocity at level $n+1$ is calculated using the pressure at level n as a predictor for the pressure at level $n+1$:

$$St\ \frac{3\boldsymbol{u}_p^{n+1} - 4\tilde{\boldsymbol{u}}^n + \tilde{\boldsymbol{u}}^{n-1}}{2\Delta t} = -\nabla p^n + \frac{1}{Re}\nabla\cdot 2\eta_p^{n+1}\boldsymbol{D}_{\boldsymbol{u}_p^{n+1}} + \frac{1}{Re\ Ca}\boldsymbol{F}_s^{n+1} \tag{14}$$

  and imposing the velocity boundary conditions of level $n+1$. The viscosity η_p^{n+1} is predicted by the extrapolation, $\eta_p^{n+1} = 2\eta^n - \eta^{n-1}$.

- By subtracting (14) from (13) and applying the divergence operator to both sides of the result, an equation for $q^{n+1} = p^{n+1} - p^n$ is obtained. It reads:

$$\nabla^2 q^{n+1} = St\ \frac{3\nabla\cdot\mathbf{u}_p^{n+1}}{2\Delta t}. \tag{15}$$

  A homogeneous Neumann boundary condition is a consistent choice for a boundary condition of (15).

- Finally, the velocity and pressure correctors at level $n+1$ are calculated according to:

$$\boldsymbol{u}^{n+1} = \boldsymbol{u}_p^{n+1} - \frac{2\Delta t\nabla q^{n+1}}{3St}, \qquad p^{n+1} = p^n + q^{n+1}. \tag{16}$$

For spatial discretization the spectral element method (Maday and Patera, 1989) is applied to obtain accurate spatial resolution. The spectral element method is a technique combining the geometrical flexibilities of the finite element method with high order accuracy of spectral methods, see Canuto *et al.* (1988). The idea is to divide a complex geometry $\boldsymbol{\Omega}$ into several spectral elements $\boldsymbol{\Omega}_k$, $1 \le k \le K$, such that

$$\bigcup_{k=1}^{K}\bar{\boldsymbol{\Omega}}_k = \bar{\boldsymbol{\Omega}} \qquad \text{and} \qquad \bar{\boldsymbol{\Omega}}_k \cap \bar{\boldsymbol{\Omega}}_l = \emptyset \text{ for all } k \neq l. \tag{17}$$

Each spectral element is mapped onto the reference element $\mathbf{\Omega}_r = [-1, 1] \otimes [-1, 1] \otimes [-1, 1]$. The global coordinates (x, y, z) are mapped to this reference element, providing the local coordinates (ξ, η, ζ) in $\mathbf{\Omega}_r$.

A Gauss-Lobatto-Legendre grid is constructed in each of the elements $\mathbf{\Omega}_k$, $1 \leq k \leq K$, where the grid G_N is a tensor product of one-dimensional Gauss-Lobatto-Legendre grids $G_N = G_{x,N} \otimes G_{y,N} \otimes G_{z,N}$, where $G_{x,N}$, $G_{y,N}$ and $G_{z,N}$ are the ordered sets $\left\{z_j | j = 0, \cdots, N\right\}$ of the roots of $(1 - z^2)\frac{d}{dz}L_n(z) = 0$, where L_n is the n^{th} order Legendre polynomial. In general, different order polynomials can be used in different directions, but throughout this paper equal orders are applied.

The velocity representation is then given by

$$u_N(x, y, z) = \sum_{i=0}^{N}\sum_{j=0}^{N}\sum_{k=0}^{N} u_{ijk}\ \phi_i(\xi)\phi_j(\eta)\phi_k(\zeta), \tag{18}$$

where the Lagrangian interpolants $\phi_i(\xi)$, $0 \leq i \leq N$ are defined on the one-dimensional reference element by the relationship

$$\phi_i(\xi) = \prod_{k \neq i}^{n} \frac{\xi - \xi_i}{\xi_k - \xi_i} = -\frac{(1 - \xi^2)}{i(i + 1)L_n(\xi_i)(\xi - \xi_i)}\frac{\partial L_n}{\partial \xi}. \tag{19}$$

Here ξ_i are the collocation points of the Gauss-Lobatto-Legendre grid $G_{x,N}$. The variables are now approximated using these Legendre Lagrangian interpolants of degree N in all three spatial directions.

Let $P^3_{N,K}(\mathbf{\Omega}_k)$ denote the space of polynomials of degree N or less in all three variables, defined in element k. The velocity and pressure fields are chosen to be in $X_N = P_{N,K}(\mathbf{\Omega}) \cap H^1_0(\mathbf{\Omega})$ with

$$P_{N,K}(\mathbf{\Omega}) = \left\{\boldsymbol{v} \in L^2(\mathbf{\Omega});\ \boldsymbol{v}|_{\mathbf{\Omega}_k} \in P^3_{N,K}(\mathbf{\Omega}_k)\right\}. \tag{20}$$

The weighted residual Galerkin formulation is now used to create a linear system of equations for the coefficients u_{ijk} similar to the finite element method. A finite element preconditioner in combination with the conjugate gradient iterative solver is applied to obtain a solution of these equations.

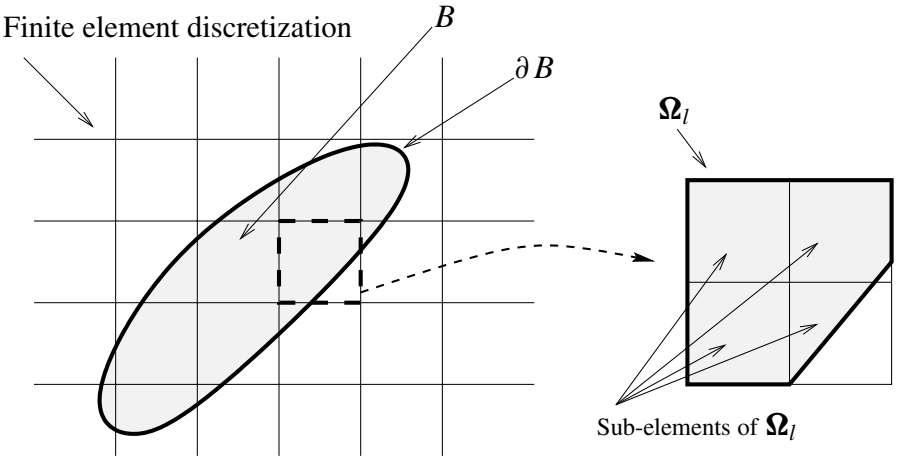

Figure 2: Graphical representation of the algorithm to construct a viscosity function. The fractions of B in the sub-elements of $\mathbf{\Omega}_l$ are used to weight the viscosity.

2.3 Including unequal viscosities

To simulate mixing of two different Newtonian fluids one needs to construct a viscosity function each time step. A straightforward technique to create this viscosity function is to determine whether or not a grid point (x_0, y_0, z_0) is inside the polygon describing the interface (Galaktionov *et al.*, 1999). The following simple algorithm can be used for this purpose. First, an auxiliary point (x^*, y^*, z^*) is chosen, which is known to be located outside the surface, and is connected by a straight line with the point (x_0, y_0, z_0). Then, the intersections of this line with a surface are found and counted. If the total number of intersections is even, the point (x_0, y_0, z_0) is outside the closed surface. If the total number of intersections is odd, it is inside.

A more elegant approach to account for the different fluids is explained in figure 2 for a two-dimensional flow problem. The extension to the full three-dimensional case is straightforward. The flow domain $\mathbf{\Omega}$ is subdivided in a number of sub-domains $\mathbf{\Omega}_l$ such that

$$\bar{\mathbf{\Omega}} = \sum_{l=1}^{L} \bar{\mathbf{\Omega}}_l \qquad \text{and} \qquad \forall_{k \neq l}\ \mathbf{\Omega}_k \cap \mathbf{\Omega}_l = \emptyset, \tag{21}$$

and the dispersed phase is represented by B and its boundary is denoted by ∂B. Note that for example in a finite element computation the sub-domains represent the elements, and in our computations the sub-domains represent the finite elements which are constructed by connecting the spectral element nodes. For each finite element $\mathbf{\Omega}_l$ the area of the intersection with the polygon ∂B is determined and used to construct a viscosity function. If this intersection exists, $\mathbf{\Omega}_l \cap B \neq \emptyset$, then the fractions of this intersection are weighted to the nodal points by subdividing the elements $\mathbf{\Omega}_l$ in four or eight (2D or 3D, respectively) sub-elements. The fractions of B in the sub-elements of $\mathbf{\Omega}_l$ are then used to weight the viscosity. Compared to the point-wise construction of the viscosity, a viscosity distribution is now constructed which is continuous across the fluid interface.

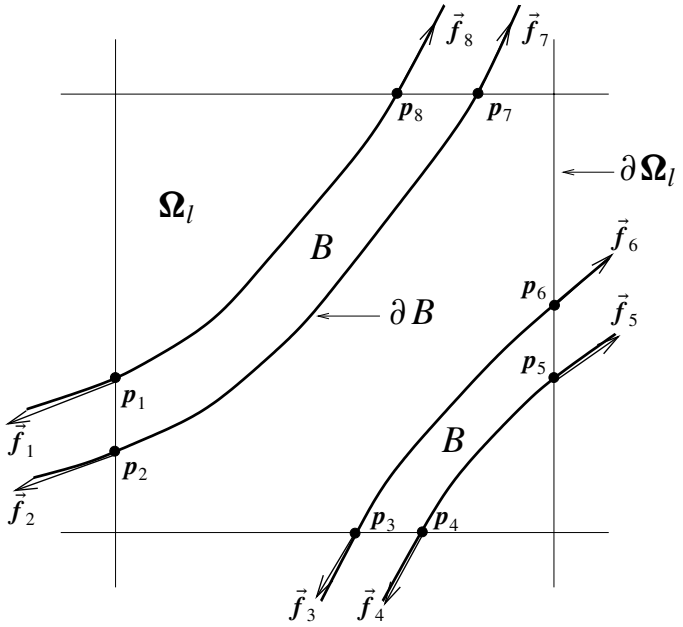

Figure 3: Components of the force, applied by surface tension to the selected rectangular volume of the fluid. Thick black lines denote the interface ∂B. The arrows show the direction of the force (tangential to the interface). For designations see text.

2.4 Including surface tension

The technique described above to construct a viscosity function can also be used to construct a "colour" function $c(\boldsymbol{x})$. If $\boldsymbol{x} \in B$ then the characteristic function $c(\boldsymbol{x})$ gets the value 1; if $\boldsymbol{x} \notin B$ then the function $c(\boldsymbol{x})$ gets the value 0. If a similar weighting is applied as for the viscosity function, c will have a smooth transition over the interface ∂B. As discussed in Brackbill *et al.* (1992), this colour function can be used to construct the surface tension volume forces $\boldsymbol{F}_s$, defined as

$$\boldsymbol{F}_s = \frac{\sigma}{\|\nabla c\|} \nabla c \, (\nabla \cdot \nabla c) \, . \tag{22}$$

Since ∇c is only non-zero in the transition region, the surface volume force also is non-zero only in the transition region. The computation of $\boldsymbol{F}_s$ via equation (22) is elegant, but also introduces some numerical problems. First, surface tension $\boldsymbol{F}_s$ is here defined through a higher-order derivative, and within the spectral element Galerkin weighted residual technique, only first-order derivatives are valid. Second, even if the spectral element discretziation is modified such that $\nabla \cdot \nabla c$ can be constructed via a valid approach, the term $\dfrac{1}{\|\nabla c\|}$ causes difficulties when $\|\nabla c\| \rightarrow 0$. Brackbill *et al.* (1992) propose some numerical techniques to bypass these difficulties. Here, a different model is used to The explicit description, via front tracking, of the shape of the interface between the two phases is used to account for surface tension in a "classical" way. Surface tension is essentially defined as a force acting on any infinitesimal piece of the contour, selected at the interface, where the interface is treated as infinitely thin. The direction of the force is tangential to the interface and normal to the contour within the interface on which it acts, while the linear density of this force is given by the surface tension coefficient. Note that the pressure difference created by the curved interface (see equation (3)) is the result of misalignment of such forces acting on neighbouring elements of the interface.

In a sharp interface model, the surface tension volume forces $\boldsymbol{F}_s$ acts as a delta function over the interface. Here, this delta function is approximated using piecewise linear functions. The finite element grid, which is constructed by connecting the spectral nodes, is used for the discretization. Surface tension forces are computed via a collocation approach, and coupled with the spectral element Galerkin weighted residual technique. A thorough numerical analysis should resolve the influence of the coupling of the piecewise linear functions to approximate the delta function with the high-order Galerkin technique. It is expected that the spectral accuracy is locally lost.

To compute the net surface tension force acting on the finite elements $\boldsymbol{\Omega}_l$ the following procedure is used:

- All the intersections p_i of the interface ∂B with the boundary of the sub-domain $\partial \boldsymbol{\Omega}_l$ are detected.
- For every intersection point p_i the local outer normal $\boldsymbol{n}_i$ to the sub-domain boundary $\partial \boldsymbol{\Omega}_l$ and the local tangent $\boldsymbol{t}_i$ to the interface ∂B are determined.
- For every point $p_i \in \boldsymbol{\Omega}_l$ the surface tension force $\boldsymbol{f}_i$ applied to the sub-domain $\boldsymbol{\Omega}_l$ is prescribed such that

$$\boldsymbol{f}_i = \pm \sigma \boldsymbol{t} \quad \text{such that} \quad \boldsymbol{f}_i \cdot \boldsymbol{n}_i > 0, \tag{23}$$

  where σ is the surface tension coefficient.

- The total surface tension force action on the sub-domain $\boldsymbol{\Omega}_l$ is defined as the vector sum

$$\boldsymbol{F}_l = \sum_{i=1}^{I} \boldsymbol{f}_i. \tag{24}$$

The specific force (per unit volume) $\boldsymbol{F}_l^*$ is found by dividing the surface tension force $\boldsymbol{F}_l$ by the volume of the sub-domain $\boldsymbol{\Omega}_l$. In case of a numerical scheme which requires that the force is prescribed at nodal or collocation points, the force $\boldsymbol{F}_l^*$ is redistributed to these points belonging to the sub-domain $\boldsymbol{\Omega}_l$, and as a result the source term $\boldsymbol{F}_s$ for equation (8) is constructed.

3 Results

The numerical scheme presented in this paper, including the strategies to include fluids with different viscosities and surface tension forces, is applied to some prototypical flows. In figure 4 a square lid-driven cavity with two different initial fluid configurations is depicted. These two prototypical configurations are considered, and the effect of viscosity ratio, and surface tension on the stretching and deformation of the interface between two viscous immiscible fluids in Stokes flow is investigated. Results are primarily presented in the form of plots of interface increase (also denoted as length stretch, see Chakravarthy and Ottino (1996)) versus time. The length of the interface between the two fluids at time t is denoted as l_t, while the initial length of the interface is defined as l_0. The length stretch is then defined as l_t/l_0. The two fluids are referred by means of subscripts "1" and "2" and the viscosity ratio is denoted as $\Lambda = \eta_1/\eta_2$. Here η_1 is the viscosity of fluid "1" and η_2 denotes the viscosity of fluid "2". The configuration with the round blob of one fluid surrounded by another fluid (figure 4) is first used to demonstrate the influence of different viscosity ratios, and later the influence of surface tension forces (using equal viscosities) is studied. In Chakravarthy and Ottino (1996) also the layered configuration, as shown in figure 4, is used to study the influence of viscosity ratios on length stretch. They were in particular interested in the difference of stretching between Λ and $1/\Lambda$. The influence of interfacial tension was neglected in their study. The layered configuration is here used to investigate this influence of interfacial forces on length stretch.

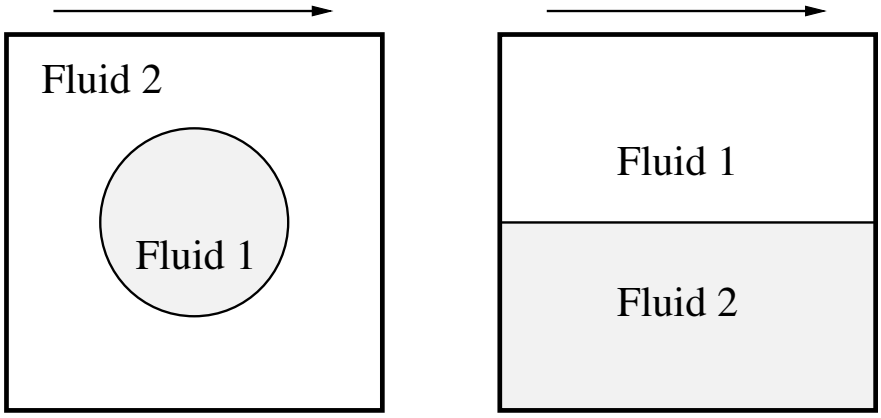

Figure 4: Mixing in a square cavity. The top wall moves to the right and two different configurations are involved in this study. On the the left the round blob case, and on the right the layered case are depicted.

In the second part of this section, it is shown that the model can be used to study drop deformation in simple flows. Examples of drop deformation are given for droplets with a viscosity different from that of the matrix fluid, where surface tension forces are negligible. Results are compared with the analytical model of Wetzel and Tucker (1999). Droplet deformation including surface tension forces can also be modelled and some results are presented.

3.1 Advection of dissimilar fluids in two-dimensional flow

3.1.1 Mixing of two fluids in a lid-driven cavity assuming negligible surface tension

A spectral element mesh consisting of 12×12 elements, each of sixth polynomial order, is used for spatial discretization of the square lid-driven cavity depicted in figure 4. Viscosity dominated flows with constant density are considered and the typical Reynolds number ($Re = \rho U L/\eta$) in cases of interest is very small, so that acceleration effects are negligible. An initial blob is placed in the centre of the cavity with radius $R = 0.25L$ where L is the width of the cavity, consisting of 100 grid points. The refinement criteria for the adaptive front tracking approach, as presented earlier in this paper, are $h_{max} = 0.1L$, $h_{c,max} = \frac{1}{2}h_{max}$, and the curvature angle α_{max} is set the 140 degrees. The integration error tolerance is set to 10^{-6}. To keep track of the history of the deformation of the blob, the previous 20 velocity fields and grid points of the blob are kept during tracking. Refinement is performed on the oldest time-level, see section 2.1.

Results for five viscosity ratios are presented in figure 5. The left column shows advection results at non-dimensionalized times 25, 50, and 75 for a blob with a five times lower viscosity compared to the bulk ($\Lambda = 1/5$). The second column on the left shows the results for $\Lambda = \frac{1}{2}$. The middle column shows the advection of a blob with a equal viscosity compared to the bulk ($\Lambda = 1$), and the fourth column shows a blob with a two times higher viscosity compared the bulk ($\Lambda = 2$). In the column on the right the advection results for a blob with a five times higher viscosity compared the bulk are presented ($\Lambda = 5$).

The length stretch versus non-dimensionalized time is graphically represented in figure 6. The area conservation is extremely good and stays within 0.005 The area conservation is extremely good and stays within 0.005 % error, indicating a proper tracking. For the five blobs a linear increase of interfacial area l_t/l_0 is observed, and the case $\Lambda = 0.2$ leads to the highest increase. The situation $\Lambda = 5$ generates less interface than the reference problem $\Lambda = 1$. An interesting phenomenon is the presence of oscillations in the l_t/l_0 curves. As stretching occurs, the blob also rotates within the cavity. Each time the blob completes a rotation, a small fold is created which causes the oscillation to appear in the l_t/l_0 curves. In Chakravarthy and Ottino (1996), the influence of the initial position on the amount of stretching was studied. For blobs which are placed slightly off centre, an increase in stretching is observed. They also studied the influence of different aspect ratios of the cavity on stretching of the interface, and showed that an increase of the cavity aspect ratio results in a decrease of interface stretching.

3.1.2 Surface tension acting on an arbitrary shaped droplet

One of the standard examples to validate a numerical code for incorporating surface tension forces is the deformation of a non-circular or non-spherical droplet. Figure 7 shows how surface tension forces act on an arbitrary shaped two-dimensional droplet (the droplet represents the Polymer Processing Society logo). The initial droplet possesses sharp corners, which usually generates difficulties for numerical methods. The coarse grain description of surface tension as discussed above experiences no difficulties from these singularities.

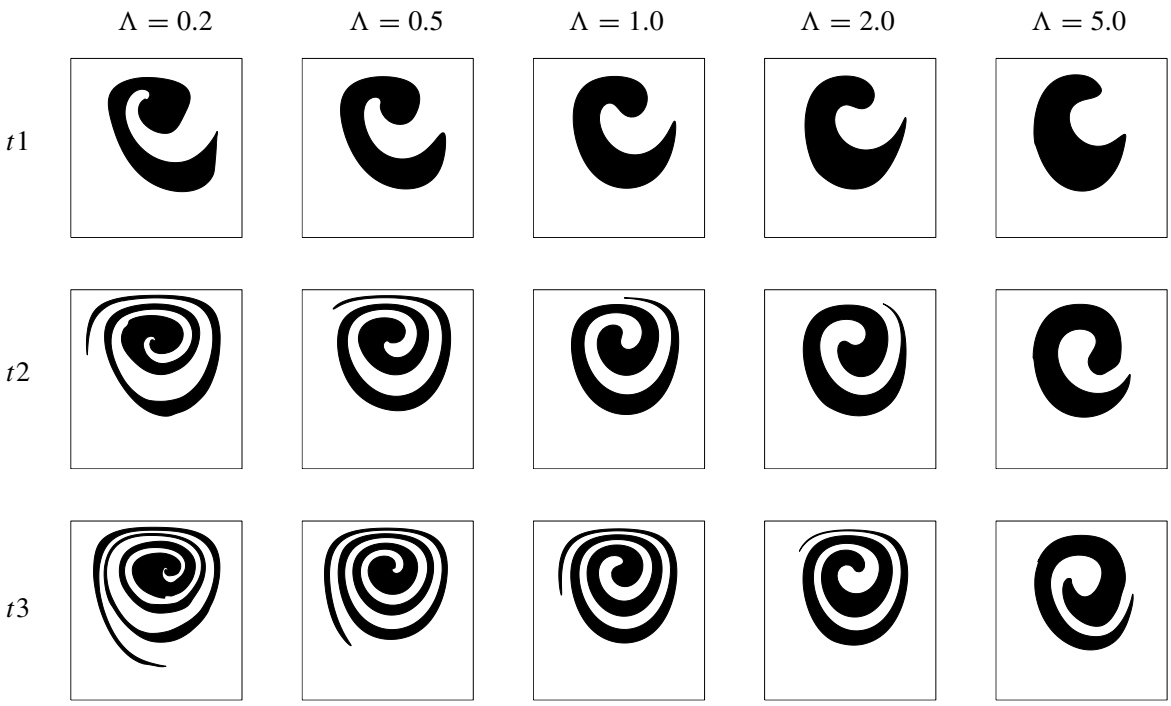

Figure 5: Advection results at times $t1 = 25, t2 = 50,$ and $t3 = 75$ for the initial blob as shown in figure 4, for five different viscosity ratios. The difference in interfacial area generation is apparent for these flows.

Two intermediate results, the pictures in the middle, show that the surface forces first act on the sharp corners, which are quickly rounded. Finally, a circular equilibrium shape results from the surface tension forces. The initial interfacial area is 6.579, and for the circular shape equals 3.007. The initial area of the blob equals 0.7112, where the final circular shape has an area equal to 0.7102. After that the kinetic energy reaches a maximum, due to the high curvature of the drop, the energy oscillates with a decreasing amplitude, and finally decays to zero. Brackbill *et al.* (1992) reports on a similar computation where an initially square drop is considered. In their computations, using the combined CSF-VOF-model, the equilibrium shape is recovered, but the interface continues to oscillate around this shape. The kinetic energy continues to oscillate and does not decay zero even after long times. The numerical dissipation in the VOF treatment provides the driving force for these oscillations.

3.1.3 Surface tension between layered fluids

In Chella and Viñals (1996), interface stretching during mixing of two fluids is investigated, using a mesoscopic description of the fluids. Their results are used here as a reference. For the layered case, as shown in figure 4, two fluids with equal viscosity and density are considered. Chella and Viñals (1996) used a special boundary condition for the moving lid to circumvent problems associated with the discontinuities in the velocity at the corners near the moving plate. For the cavity with width L they applied the function

$$u(x) = U_0 x^2 (1 - (x/L))^2 \tag{25}$$

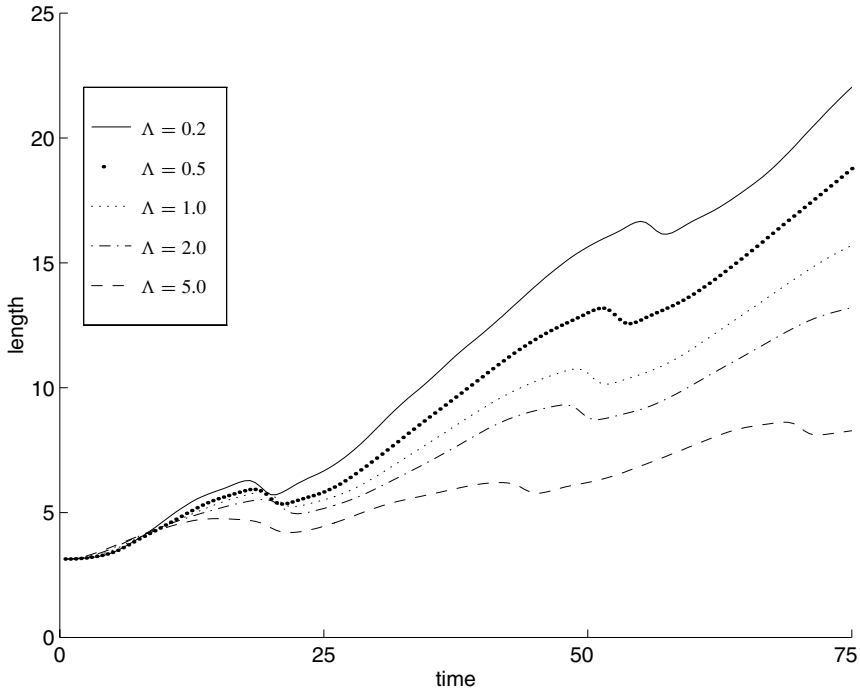

Figure 6: Increase in interfacial tension for the blobs as initially shown in figure 4 for five different viscosity ratios.

as boundary condition, which is also chosen in this section. The parameters L and U_0 are both chosen equal to 1. Equation (25)is used here to allow a comparison of the diffuse interface results of Chella and Viñals (1996) with the sharp interface technique presented here. The algorithm described in the previous section is used to follow the evolution of the active interface. A spectral element mesh consisting of 16×16 elements, each of sixth polynomial order, is used for spatial discretization of the square lid-driven cavity depicted in figure 4. The time-step used for integration is $\Delta t = 0.005$. At $t = 0$ the steady velocity and pressure fields are imposed, corresponding to the boundary condition for the lid as defined in equation 25.

The evolution of the interface at various times is depicted in figure 8 for two different capillary numbers, $Ca = 0.1$ and $Ca = 1$, here defined as $Ca = \eta U_0/\sigma$. Chella and Viñals (1996) used a slightly different definition of the capillary number related to the length scale of the diffuse interface. The characteristic velocity U_0 is set equal to 1. The figure clearly shows that, for a lower capillary number, the stretching of the interface is considerably lower. Moreover, if the second fluid (bottom layer) reaches the centre of the cavity, the capillary forces are larger than the viscous forces and a

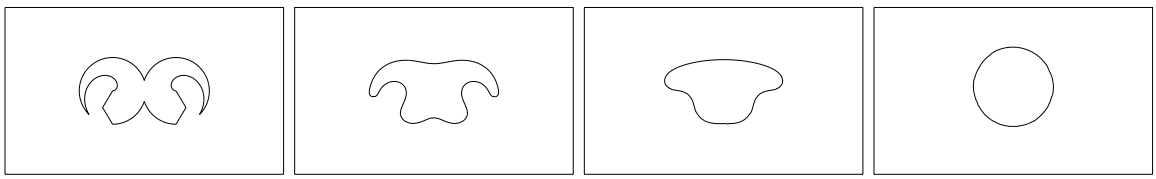

Figure 7: Surface tension is acting on a complex shaped droplet (PPS logo). Despite of the complicated geometrical shape, surface tension forces deform the blob towards a circular shape.

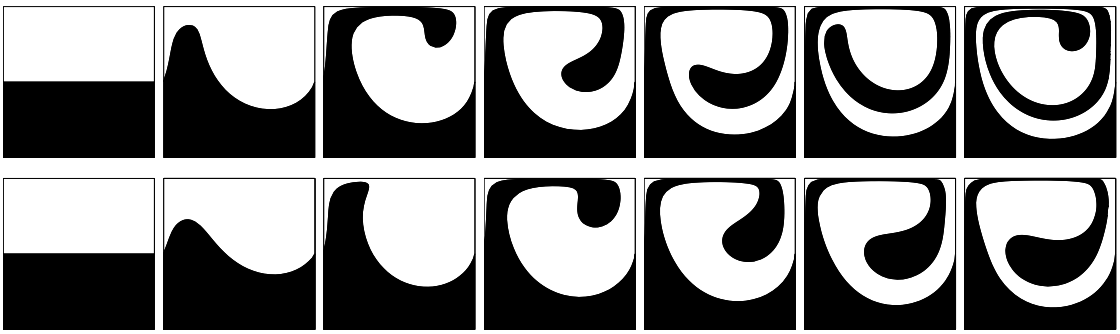

Figure 8: Top row corresponds to the case $Ca = 1$, where the bottom row depicts $Ca = 0.1$. The figures show the evolution of the interface at various times.

circular shape of the interface is enforced. These results show good qualitive agreement with the results obtained by the diffuse interface technique of Chella and Viñals (1996). The stretching of the interface is lower for $Ca = 0.1$ than for $Ca = 1$, which is again less than for a passive interface deformation neglecting surface tension.

3.2 Droplet deformation

To understand how the structure in inhomogeneous fluids evolve during flow, many experimental and theoretical studies have reported on the deformation and breakup of small droplets suspended in simple flows. These studies included effects such as interfacial tension, unequal viscosities, and fluid elasticity. Stone's review on this topic mentions the most important results. Although this subject was not a main objective of this paper, the models presented in this work can be applied to study droplet deformation. For example, transient effect in fully three-dimensional flows can be studied, or droplet relaxation after the flow is stopped.

Recently, a numerical model has been proposed by Christini *et al.* (1998), who performed fully three-dimensional calculations of droplet deformation and found excellent agreement with experimental data. They used an adaptive mesh refinement technique to study complex shapes approaching breakup. Wetzel and Tucker (1999) introduced the droplet shape tensor and developed the mathematical tools to treat single droplets without interfacial tension in general three-dimensional flows. Results presented in that work are used here to validate our model.

To demonstrate (or validate) that the model presented in this paper can be used to study droplet deformation, deformation in two different regimes is examined. In the first regime, interfacial forces are assumed to be negligible, but unequal viscosities of the drop and the matrix fluid are permitted. Here, there is no relaxation or breakup, and the drop maintains an ellipsoidal shape. In the second regime, significant interfacial tension is allowed. The droplet deformation is influenced by the capillary forces, and the drop can breakup into smaller droplets.

3.2.1 Droplet deformation for $Ca \gg 1$

In simple shear the deformation of an initially spherical droplet is studied for different viscosity ratios Λ, i.e., $\Lambda = 0.1,\ 1,$ and 10. The results are presented by comparing the axis ratios from our model with the theory of Wetzel and Tucker (1999). For $\Lambda \leq 3$ the droplet stretches indefinitely, and in cases where $\Lambda \geq 5$ the droplet tumbles. The theory of Wetzel and Tucker (1999) predicts that, in the absence of interfacial tension, an initially spherical droplet of sufficient high viscosity ratio will

tumble indefinitely. If surface tension forces are present in the system then the tumbling will be damped, and a stationary droplet shape can be reached.

First, a viscosity ratio $\Lambda = 10$ is considered neglecting interfacial tension, and the calculations are continued to a maximum strain of 15. The domain between the two moving plates is discretized into $24 \times 8 \times 8$ spectral elements of fourth order in each direction. The initially spherical blob with radius R is placed in the centre of the domain, and $R = 0.2 \times H$, where H is the height between the two plates. The refinement criteria, for the adaptive front tracking approach, as presented in section 2.1, are $h_{max} = 0.05R$, $h_{c,max} = \frac{1}{2}h_{max}$, and the curvature angle α_{max} is set the 40 degrees. The integration error tolerance is set to 10^{-5}, and to keep track of the history of the deformation of the blob, the previous five velocity fields and grid points of the blob are stored during tracking. Refinement, as the blob stretches, is performed on the oldest time-level, see section 2.1.

The computations for $\Lambda = 10$ using the model presented in this paper show that the blob tumbles, and the orientation angle of the droplet major axis is given in figure 9. The results of Wetzel and Tucker (1999) are added as a reference, and it is observed that the model presented here shows a reasonable equivalence. The scaled width of the blob, denoted as b/R similar to Wetzel and Tucker (1999), as a function of the strain is studied and the results are given in figure 9.

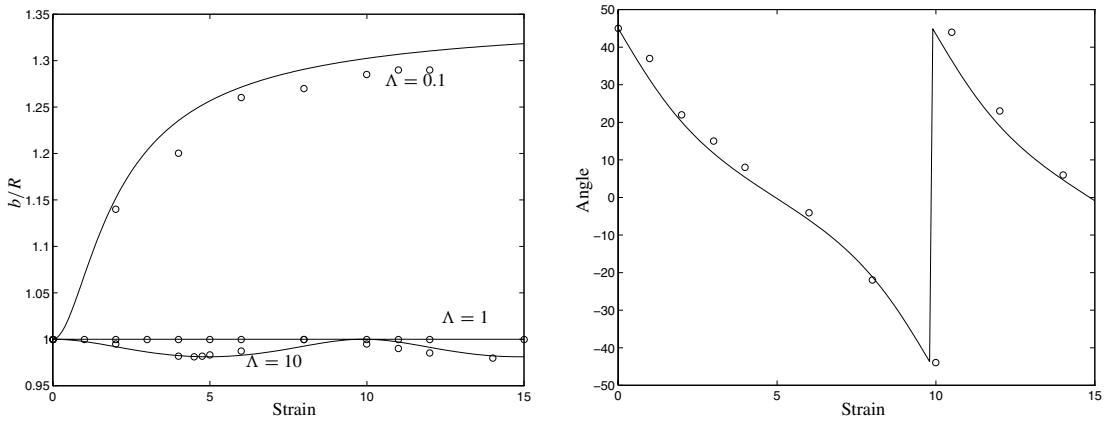

Figure 9: The figure on the left show the width of the drop for different viscosity ratios and as function of strain. The figure on the right displays the drop angle for the case $\Lambda = 10$. The solid lines are results by Wetzel and Tucker (1999), and the circles denotes the present solution.

For a viscosity ratio $\Lambda = 1$ the droplet width is constant during stretching, where for a viscosity ratio $\Lambda = 0.1$, and again neglecting interfacial tension, the drop stretches infinitely, and the drop *increases* in width as it stretches. Similar effects have been seen experimentally in viscoelastic flows, and were attributed to normal stress differences Levitt and Macosko (1996). These result show that droplet widening can also occur in purely Newtonian systems, even without interfacial tension, and that the droplet experiences three-dimensional deformation. These results were also reported and discussed in Wetzel and Tucker (1999), and they found that for $\Lambda < 1$ the drop widens.

3.2.2 Droplet deformation for $Ca < 10$

Interfacial tension forces cannot be neglected if the capillary number is small enough, and solutions of the full three-dimensional problem including surface tension are required. Compared to the previous section, now the surface tension forces are computed each time step. An extension of the technique to the full three-dimensional problem is straightforward. The main difference is that here intersections of

three-dimensional objects, described by polyhedrons, are required at two instances: first, to construct a viscosity function, and second, to compute the surface tension forces by determining the intersections between the interfaces and the finite elements. In the current programming model this is accomplished at once, and no substantial additional costs result from including surface tension forces. In general however, computations including surface tension forces *are* more time consuming, because of the time-step restriction constrained by these forces.

One example is given where surface tension is included, where the deformation of a droplet is studied under shear. During stretching it is observed that the blob loses its ellipsoidal shape, and appears like an "S". This is exactly the droplet shape as observed in other studies, see Stone (1994) and references therein.

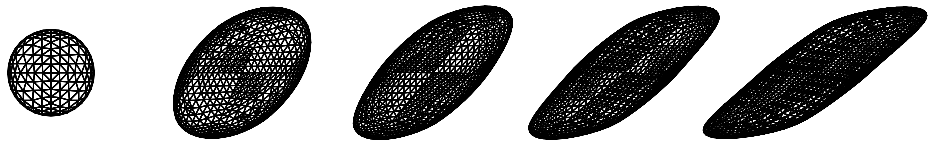

Figure 10: Droplet deformation for $Ca = 1$; the drop looses its ellipsoidal shape as a result from the surface tension forces and a S-like shape is formed.

4 Conclusions

As opposed to the case of single-phase mixing, the stretching and deformation of interfaces between two fluids is a more difficult problem to model, even in a prototypical system like a cavity flow. The non-periodic nature of the flow and the assembly of parameters and initial conditions make results hard to generalize. Computations usually require more CPU time and system resources.

A model is presented to study multi-component mixing flows, allowing unequal viscosities and surface tension forces. This model uses a fixed grid to compute the velocity field, and a variable adaptive grid to track the interfaces. The model interprets surface tension as a continuous, three-dimensional effect across an interface, rather than as a boundary condition on the interface. The model is general and can be straightforwardly extended to different geometries, or to include fluids of different rheology. Here only results in simple domains concerning Newtonian fluids are presented.

The results roughly cover two parts. In the first part, mixing of two immiscible fluids in a two-dimensional cavity flow was considered. Two configurations were studied; the first consists of two layers of dissimilar fluids in a lid-driven cavity. The second deals with a round blob placed in the centre of the lid-driven cavity. In the second part some examples of drop deformation in shear flow were give, demonstrating that the model can be used for this purpose.

For both configurations in the first part, the influence of surface tension forces on the generation of interfacial area was studied. It is observed that surface tension forces tend to inhibit the generation of interfacial area. The lower the capillary number the lower the increase in interfacial area. For the round blob case, for a capillary number of $Ca = 0.5$, the viscous forces are not large enough to stretch

the interface. The blob is modified by the flow, and eventually reaches a steady shape, where the blob merely rotates. For the round blob the effect of different viscosity ratios was also considered. For viscosity ratios less than one, so where the blob has a lower viscosity than the matrix fluid, the blob generates more interface compared to the equal viscosity system. For viscosity ratios larger than one the opposite is true: the blobs stretches less easily, and for large enough ratios the blob acts like a solid obstacle. The studies performed for the two-dimensional cavity flow with the layered or round blob configuration can be easily extended to three dimensions. However, the motion remains quasi-two-dimensional, and the effects resulting from a viscosity ratio different to one are similar to the two-dimensional case.

Finally, a three-dimensional application of the model is presented where droplet deformation in simple shear is considered. For $Ca \gg 1$, surface tension forces are negligible, results were compared with the analytical model of Wetzel and Tucker (1999). For three different viscosity ratios, $\Lambda = 10,\ 1,$ and 0.1, the width of blob as a function of strain is compared with results obtained by Wetzel and Tucker (1999). In all cases a good equivalence was observed. Furthermore, the deformation of a single drop under shear is presented where $Ca = 1$. Here, the initial ellipsoidal shape of the drop is destroyed and a S-like shape is observed.

References

Anderson, D.M., McFadden, G.B., and Wheeler, A.A. (1998). Diffuse-interface methods in fluid mechanics. *Annu. Rev. Fluid Mech.*, **30**, 139–165. 2

Anderson, P.D., Galaktionov, O.S., Peters, G.W.M., van de Vosse, F.N., and Meijer, H.E.H. (1999). Analysis of mixing in three-dimensional time-periodic cavity flows. *J. Fluid Mech.*, **386**, 149–166. 1

Aref, H. (1984). Stirring by chaotic advection. *J. Fluid Mech.*, **143**, 1–21. 1

Ashwin, P. and King, G.P. (1997). A study of particle paths in non-axisymmetric Taylow-Couette flows. *J. Fluid Mech.*, **338**, 341–362. 1

Batchelor, G.K. (1967). *An Introduction to Fluid Mechanics*. Cambridge University Press. 2

Beris, A.N., Richard, J.R., and Lenhoff, A.M. (1996). A Volume of Fluid Method Applied to Liquid-Liquid Jet Breakup and Drop Dynamics. In Y. Y. Renardy and A. V. Coward, editors, *Proceedings in Applied Mathematics*, chapter 4, pages 349–367. SIAM, Philidelphia. 2.1

Brackbill, J.U., Kothe, D.B., and Zemach, C. (1992). A continuum model for modeling surface tension. *J. Comp. Phys.*, **100**, 335–354. 2, 2, 2.4, 2.4, 3.1.2

Canuto, C., Hussaini, M.Y., Quarteroni, A., and Zang, T.A. (1988). *Spectral methods in fluid dynamics*. Springer−Verlag, New York, Berlin. 2.2

Carey, G.F. and Chen, Y. (1995). Simulation of Fluid Mixing Using Least-Squares Finite Elements & Particle Tracing. *Int. J. Num. Heat & Fluid Flow*, **5**. 1

Chakravarthy, V.S. and Ottino, J.M. (1996). Mixing of two viscous fluids in a rectangular cavity. *Chem. Eng. Sci.*, **51**, 3613–3622. 1, 3, 3, 3.1.1

Chella, R. and Viñals, J. (1996). Mixing of two-phase fluid by cavity flow. *Phys. Rev. E*, **53**(4), 3832–3840. 1, 2, 3.1.3, 3.1.3, 3.1.3, 3.1.3, 3.1.3

Chien, W.L., Rising, H., and Ottino, J.M. (1986). Laminar Mixing and Chaotic Mixing in Several Cavity Flows. *J. Fluid Mech.*, **170**, 355–377. 1

Christini, V., Blawzdzieweicz, J., and Loewenberg, M. (1998). Drop breakup in three-dimensional viscous flows. *Phys. Fluids*, **10**, 1781–1783. 3.2

Galaktionov, A.S., Anderson, P.D., and Peters, G.W.M. (1997). Mixing simulations: tracking strongly deforming fluid volumes in 3D flows. In M. Bubak, J. Dongarra, and J. Wasniniewski, editors, *Recent advances in Parallel Virtual Machine and Message Passing Interface*, volume 1332 of *Lecture Notes in Computer Science*, pages 463–469. Springer. 2.1.1

Galaktionov, O.S., Anderson, P.D., Peters, G.W.M., and Vosse, F.N. van de (1999). An adaptive front tracking technique for three-dimensional transient flows. *Int. J. Numer. Meth. Fluids*. (submitted). 2.1, 2.3

Geist, A., Beguelin, A., Dongarra, J., Jiang, W., Manchek, R., and Sunderman, V. (1994). *PVM: Parallel Virtual Machine. A user's guide and tutorial for networked parallel computing*. The MIT Press, Cambridge, Massachusetts. 2.1.1

Harlow, F.H. and Welch, J.E. (1965). Numerical calculation of time-dependent viscous incompressible flow of fluid with free-surface. *Phys. Fluids*, **8**, 2182–2189. 2

Hirt, C.V. and Nichols, B.D. (1981). Volume of fluid (VOF) methods for the dynamics of free boundaries. *J. Comput. Phys*, **39**, 201–225. 2, 2.1

Hyman, J.M. (1984). Numerical methods for tracking interfaces. *Physica D*, **12**, 396–407. 2.1, 2.1

Landau, L.D. and Lifshitz, E.M. (1959). *Fluid Mechanics*. Pergamon, New York. 2, 2

Levitt, L. and Macosko, C.W. (1996). Influence of normal stress difference on polymer drop deformation. *Polym. Eng. Sci.*, **36**, 1647–1655. 3.2.1

Liu, M., Peskin, R.L., Muzzio, F.J., and Leong, C.W. (1994). Structure of Stretching Field in Chaotic Cavity Flows. *Aiche*, **40**(8), 1273–1286. 1

Maday, Y. and Patera, A.T. (1989). Spectral element methods for the incompressible Navier−Stokes equations. In A. Noor, editor, *State-of-the-Art surveys on computational mechanics*. ASME, New York. 2.2

Noh, W.F. and Woodward, P. (1976). SLIC (simple line interface calculation). In A. I. Dooren and P. J. Zandbergen, editors, *Fifth Int. Conf. on Numerical Methods in Fluid Dynamics*, volume 59 of *Lecture Notes in Physics*, pages 330–340, Berlin. Springer. 2.1

Ottino, J.M. (1989). *The kinematics of mixing: stretching, chaos and transport*. Cambridge University Press. 1

Qu, X. and Li, X. (1996). A 3D surface tracking algorithm. *Comput. Vision Graphics Image Process.*, **64**, 147–156. 2.1

Rudman, M. (1997). Volume-tracking methods for interfacial flow calculations. *Int. J. Heat & Fluid Flow*, **24**, 671–691. 2.1, 2.1

Stone, H.A. (1994). Dynamics of droplet deformation and breakup in viscous fluids. *Annu. Rev. Fluid Mech.*, **26**, 65–102. 3.2.2

Tryggvason, G. and Unverdi, S.O. (1990). Computations of three-dimension Rayleigh-Taylor instability. *Phys. Fluids A*, **5**, 656–659. 2.1

Unverdi, S.O. and Tryggvason, G. (1992a). Computations of multi-fluid flow. *Phys. Fluids D*, **60**, 70–83. 2.1, 2.1

Unverdi, S.O. and Tryggvason, G. (1992b). A front-tracking method for viscous, incompressible Multi-fluid flows. *J. of Comp. Phys.*, **100**, 25–37. 2, 2, 2.1

Verschueren, M. (1999). *A diffuse-interface model for structure development during flow*. Ph.D. thesis, Eindhoven University of Technology, The Netherlands. 2

Wetzel, E.D. and Tucker, C.L. (1999). Droplet deformation in dispersions with unequal viscosities and nehligible interfacial tension. *J. Fluid Mech.* Submitted. 3, 3.2, 3.2.1, 3.2.1, 3.2.1, 3.2.1, 9, 3.2.1, 4, 4

Young, S. S., White, J. J., Clark, E. S., and Oyanagi, Y. (1980). A basic eperimental study of sandwich injection molding with sequential injection. *Pol. Eng. Sci.*, **20**, 798–804. 2.1

Zhang, D.F. and Zumbrunnen, D.A. (1996a). Influences of Fluidic Interfaces on the formation of fine scale structures by chaotic mixing. *Journal of Fluids Engineering, Transactions of ASME*, **118**, 40–47. 1

Zhang, D.F. and Zumbrunnen, D.A. (1996b). Chaotic mixing of two similar fluids in the presence of a third dissimilar fluid. *AIChE Journal*, **42**(12), 3301–3309. 1